European Cells and Materials Vol.54 2025 (pages 115–127) DOI: 10.22203/eCM.v054a08 ISSN 1473-2262

Original Article

WNT/β-CATENIN-MEDIATED OSTEOGENIC REPAIR OF OSTEOPOROTIC DEFECTS BY DICALCIUM SILICATE-ACTIVATED BMSCS IN RATS

X. Zhang[1,*], Q. Zhang[2], B.Y. Zhu[3] and R. Li[3]

[1]Department of Oral Medicine, The First Affiliated Hospital of Zhengzhou University, 450052 Zhengzhou, Henan, China
[2]Department of Pediatric Dentistry, Zhejiang Provincial Stomatological Hospital, 310006 Hangzhou, Zhejiang, China
[3]Department of Oral and Maxillofacial Surgery, The First Affiliated Hospital of Zhengzhou University, 450052 Zhengzhou, Henan, China

Abstract

Background: Osteoporosis is a metabolic bone condition that increases fracture risk. This study aimed to examine whether dicalcium silicate (C_2S) promotes bone-forming potential of bone marrow mesenchymal stem cells (BMSCs) via Wnt/*β-catenin* signaling pathway and enhances bone repair in osteoporotic rats. **Methods:** Rat BMSCs were isolated and identified. Cell counting kit-8 method was employed to evaluate proliferation of BMSCs. BMSCs were divided into control, C_2S, and C_2S + Wnt inhibitor (Dickkopf-1 (DKK-1)) groups. Mineralization was evaluated through alizarin red staining. Quantitative real-time polymerase chain reaction (PCR) and western blot assays were conducted to assess messenger ribonucleic acid (mRNA) and protein levels of *β-catenin*, Runt-related transcription factor 2 (*Runx2*), osteopontin (*OPN*), and osteocalcin (*OCN*). An osteoporotic bone defect rat model was established. The animals were randomly divided into model, BMSC, and C_2S-BMSCs groups. Bone regeneration was analyzed via micro-computed tomography (CT) and histological staining. Immunohistochemistry analyzed *β-catenin*, *Runx2*, *OPN*, and *OCN* expressions in femur tissues. **Results:** BMSCs were successfully isolated and identified. 100 μg/mL C_2S was used for subsequent experiments. *In vitro*, C_2S significantly increased mineralized nodule formation and increased the mRNA and protein levels of *β-catenin*, *Runx2*, *OPN*, and *OCN* ($p < 0.001$). These effects were considerably attenuated by DKK-1 ($p < 0.01$). *In vivo*, BMSCs and C_2S-BMSC scaffolds improved bone regeneration, with C_2S-BMSCs having better repair effects ($p < 0.01$), and higher expressions of *β-catenin*, *Runx2*, *OPN*, and *OCN* ($p < 0.05$) than BMSCs. **Conclusions:** C_2S-induced stimulation of Wnt/*β-catenin* pathway stimulates BMSC osteogenesis, thereby facilitating osteoporotic bone regeneration and offering a promising therapeutic approach for osteoporosis-related bone defects.

Keywords: Dicalcium silicate, osteoporosis, mesenchymal stem cells, osteogenesis, Wnt signaling pathway.

***Address for correspondence**: X. Zhang, Department of Oral Medicine, The First Affiliated Hospital of Zhengzhou University, 450052 Zhengzhou, Henan, China. Email: 15238075169@163.com.

Introduction

Osteoporosis, a widespread bone condition characterized by weakened bone strength and disrupted bone microarchitecture, poses a major health challenge worldwide, especially in older adults [1]. Individuals with this disease are prone to fragility fractures and impaired bone healing, with osteoporotic bone defects creating particular clinical challenges due to decreased osteogenic potential and disturbed bone remodeling [2]. Studies in epidemiology indicate that osteoporosis affects 18.3 % of the global population [3], with 44.3 % of those with osteoporosis potentially experiencing a fragility fracture over the next 10 years [4]. Current therapeutic methods, including self-donated bone grafts and man-made bone alternatives, are somewhat useful but are restricted by donor site morbidity, limited supply, and poor integration in osteoporotic conditions [5,6]. These restrictions have generated significant research efforts toward creating bioactive materials that can actively enhance osteogenesis and facilitate bone regeneration in compromised skeletal areas.

Bone marrow mesenchymal stem cells (BMSCs) play a pivotal role in bone regeneration through their osteogenic differentiation potential [7]. In osteoporosis, this capacity is significantly impaired due to aging, hormonal imbalances, chronic inflammation, and metabolic dysfunction, leading to reduced bone mineral density (BMD), compromised bone microarchitecture, and a greater likelihood of fragility fractures [8]. Notably, BMSC differentiation into bone-forming cells is tightly controlled by critical signaling pathways, particularly the Wnt/*β-catenin* signaling path-

way [9,10]. BMSCs have a diminished capacity for bone formation in osteoporotic conditions, partly because of the dysregulation of essential signaling mechanisms such as the Wnt/*β-catenin* signaling pathway [11]. The canonical Wnt/*β-catenin* pathway serves as a master regulator of skeletal homeostasis. Upon Wnt ligand binding to Frizzled receptors, *β-catenin* escapes proteasomal degradation, accumulates in the cytoplasm, and translocates to the nucleus to activate osteogenic transcription factors such as Runt-related transcription factor 2 (*Runx2*) and Osterix while suppressing adipogenic peroxisome proliferator-activated receptor gamma (PPARγ) expression [12]. This dual function maintains the osteoblast-adipocyte balance in bone marrow niches. The Wnt/*β-catenin* pathway is crucial for bone formation, as its activation encourages osteoblast differentiation and bone growth, whereas its inhibition leads to bone loss [13]. The crucial function of this pathway in maintaining bone homeostasis makes it a promising target for treatments designed to improve bone regeneration in osteoporosis [14]. In osteoporosis, elevated levels of Wnt inhibitors (e.g., sclerostin and Dickkopf-1 (Dkk-1)) lead to *β-catenin* depletion and subsequent suppression of osteoblast differentiation [15,16]. Preclinical study has demonstrated that pharmacological activation of Wnt/*β-catenin* signaling can rescue BMSC differentiation defects and reverse bone loss in osteoporotic models [17].

Dicalcium silicate (Ca_2SiO_4, C_2S), a type of calcium silicate-based biomaterial, has attracted increasing attention in bone regeneration applications owing to its known biocompatibility and bone-forming capabilities [18,19]. Research has previously indicated that C_2S releases biologically active ions (Ca^{2+} and SiO_3^{2-}) to encourage the growth and specialization of osteoblasts [20,21]. Notably, C_2S has yielded positive results in fostering angiogenesis and bone repair in cell and animal models [22,23]. While C_2S has potential for bone regeneration, its standalone application exhibits limited efficacy for addressing critical-sized defects or compromised osteogenic microenvironments, as evidenced by studies highlighting its insufficient restoration capacity in osteoporotic bone [24]. This limitation underscores the urgent need for the development of combinatorial strategies to increase its therapeutic efficacy, particularly in pathological bone microenvironments characterized by impaired regenerative capacity. Luo *et al.* [25] demonstrated the pro-osteogenic effects of C_2S on BMSC differentiation; however, the precise molecular mechanisms involved remain incompletely understood. Specifically, the potential regulatory role of C_2S in regulating the Wnt/*β-catenin* pathway cascade during BMSC osteogenesis warrants further investigation. Moreover, a thorough examination is necessary to evaluate the therapeutic effectiveness of C_2S in repairing osteoporotic bone defects.

We aimed to comprehensively analyze the osteoinductive influence of C_2S in BMSCs, elucidate its molecular mechanisms, and assess its therapeutic potential in addressing bone defects caused by osteoporosis in rats. Our results demonstrated that C_2S potentiated BMSC osteogenesis through Wnt/*β-catenin* signaling pathway activation and improved their efficacy in repairing osteoporotic femoral defects in osteoporotic rats.

Materials and Methods

Preparation of C_2S Particles and Scaffolds

High-purity C_2S particles (GA09300) (99 %) were synthesized using the sol-gel method and provided by Shanghai Institute of Ceramics, Chinese Academy of Sciences (Shanghai, China), as described previously [26]. Haiao® oral rehabilitation membranes (240618, material: collagen; porosity: 85 %; degradation rate: ~ 12 %/month, provided by the manufacturer and verified via pilot testing, ZH-BIO, Yantai, China) were used as collagen-based scaffolds as previously reported [22]. The membranes were crafted into a circular thin sheet with a diameter of approximately 5 mm using a 5 mm hole punch. To prepare the scaffolds, the BMSCs were exposed to phosphate-buffered saline (PBS) or 100 μg/mL C_2S for 72 h each. The scaffolds (5×5 mm^2) were prewetted in serum-free medium for 1 h at 37 °C. A total of 5×10^5 cells/scaffold (in 50 μL of complete medium) were drop-seeded (5×10 μL aliquots) at 15-min intervals for absorption. After 2 h of adhesion, the scaffolds were transferred to 24-well plates with 1 mL of medium to create BMSCs and C_2S-BMSC scaffolds. The cell attachment efficiency was confirmed to be >90 % by a live/dead assay.

BMSC Isolation, Culture, and Identification

Four-week-old rats were intraperitoneally injected with 150 mg/kg of 1 % sodium barbiturate (11715, Sigma-Aldrich, Merck, St. Louis, MO, USA) for euthanasia. Subsequently, the femurs were dissected, and the bone marrow was flushed with alpha-minimum essential medium (α-MEM) (12571063, Gibco, Thermo Fisher Scientific, Waltham, MA, USA) to rinse the marrow cavity repeatedly. The cell suspensions were filtered to remove tissue fragments, followed by centrifugation at 1000 r/min for 5 min. The supernatants were discarded, and the cell pellets were reconstituted in α-MEM containing 10 % fetal bovine serum (FBS) (A5670701, Gibco) and 1 % penicillin/streptomycin (15140122, Gibco). Subsequently, the cells (6×10^6 cells/mL) were plated in culture dishes and maintained at 37 °C under 5 % CO_2. When the cells reached approximately 80 % confluence, subculturing was performed. The cell morphology was viewed under a microscope (XD-202, NOVEL, Nanjing, China). Further experiments utilized cells between passages 3 and 5.

Detection of Mycoplasma Contamination

Following isolation and characterization, BMSCs were tested for mycoplasma contamination using the Venor® GeM Classic detection kit (11-1100G, Minerva-Biolabs, Berlin, Germany) according to the manufacturer's instructions. In brief, 100 μL of BMSC supernatant was processed with proteinase K, amplified by polymerase chain reaction (PCR) (40 cycles), and analyzed by electrophoresis (270 bp = positive).

Cell Treatment and Grouping

First, BMSCs were treated with different doses of C_2S (0, 25, 50, 100, and 200 μg/mL) for 12, 24, 48, 72 h, or 7 d. Second, the BMSCs were divided into three groups: the control group, the C_2S group, and the C_2S + DKK-1 group. C_2S group cells were exposed to 100 μg/mL of C_2S. Cells in the C_2S + DKK-1 group were pretreated with 0.5 μg/mL DKK-1 (371208, Sigma-Aldrich) for 1 h, followed by 100 μg/mL C_2S treatment.

Flow Cytometry

Third-passage (P3) BMSCs, which reached 80–90 % confluency, were detached using 0.25 % trypsin and centrifuged to obtain cell pellets. The resulting cell suspension was adjusted to 1×10^5 cells/mL. To assess surface marker expression, the cells were treated with PE-labeled CD90 (MA5-17750), CD105 (MA5-46823), CD73 (MA5-38752), and CD45 antibodies (25-0451-82, Invitrogen, Thermo Fisher Scientific) for 30 min in the dark. Affinity-purified rat immunoglobulin G (IgG) antibody (11036D, Invitrogen) served as an isotype control. Cell sorting using fluorescence activation was performed with flow cytometry (CytoFLEX, Beckman Coulter, Brea, CA, USA), followed by data processing using FlowJo software (V10.10, Tree Star, Ashland, OR, USA).

Alizarin Red Staining

Alizarin red staining was conducted to evaluate the osteogenic differentiation of the BMSCs. For cell identification, osteogenic induction medium (OIM) was prepared with α-MEM plus 10 % FBS, 1 % penicillin/streptomycin, 0.01 μmol/L dexamethasone (A13449, Thermo Fisher Scientific, Waltham, MA, USA), 10 mmol/L β-glycerophosphate (G1485, Solarbio, Beijing, China), and 50 mg/L ascorbic acid (A8100, Solarbio, Beijing, China). BMSCs were plated in 24-well plates at 1×10^4 cells/well for 24 h, and the medium was changed to OIM and maintained for 2 weeks, with fresh medium provided every other day. After being fixed with 4 % paraformaldehyde for 30 min, the cells were incubated with alizarin red solution (ALIR-10001, Cyagen Biosciences, Suzhou, China) for 10 min. The mineralization patterns were documented using a microscope (CKX53, Olympus, Tokyo, Japan).

Table 1. qRT–PCR primer sequences.

Gene	Prism sequences (5′–3′)
β-catenin-F	TGGAGCACGCACAGATAGGT
β-catenin-R	CAACAAGCCCTCTCGATGGT
Runx2-F	TCGCCTCACAAACAACCACA
Runx2-R	AGGCTGTTTGACGCCATAGT
OPN-F	TCTCTCAGAAGCAACCACCAC
OPN-R	TCATTGCTCTGATGGGGAGC
OCN-F	AAGTCCCACACAGCAACTCG
OCN-R	TCCATTGTTGAGGTAGCGCC
GAPDH-F	TGTCTCCTGCGACTTCAACA
GAPDH-R	GGTGGTCCAGGGTTTCTTACT

Oil Red O Staining

Adipogenic induction medium (AIM) was prepared with α-MEM plus 10 % FBS, 1 % penicillin/streptomycin, 0.5 mM isobutylmethyl xanthine (410957, Sigma-Aldrich), 1 μM dexamethasone (A13449, Thermo Fisher Scientific, Waltham, MA, USA), 10 μg/mL insulin (15523, Sigma-Aldrich), and 100 μM indomethacin (405268, Sigma-Aldrich). To induce osteogenesis, for adipogenic differentiation, BMSCs were cultured with AIM for 14 days and stained with oil red O solution (G1262, Solarbio, Beijing, China). The stained sections were photographed under a microscope (CKX53, Olympus, Tokyo, Japan).

Cell Counting Kit-8 (CCK-8) Assay

After 24 h of BMSC (6000 cells/well) seeding in 96-well plates, the cells were exposed to varying doses of C_2S (0, 25, 50, 100, and 200 μg/mL). After 12, 24, 48, 72 h, and 7 d of C_2S exposure, 10 μL of CCK-8 solution (G4103, Servicebio, Wuhan, China) was added. The absorbance at 450 nm was recorded with a microplate reader (CMax Plus, Molecular Devices, San Jose, CA, USA) after 3 h of incubation at 37 °C.

Quantitative Real-Time PCR (qRT-PCR)

Using TRNzol Universal Reagent (DP424, TIANGEN, Beijing, China), BMSC RNA extraction was conducted, and complementary deoxyribonucleic acid (cDNA) was generated using a FastQuant cDNA First Strand Synthesis Kit (KR108, TIANGEN, Beijing, China). Quantitative polymerase chain reaction (qPCR) was conducted using SuperReal PreMix Plus (SYBR Green) (FP206, TIANGEN, Beijing, China) and amplified on a LightCycler96 real-time PCR system (LightCycler96, Roche, Basel, Switzerland). The prism sequences were synthesized by GENCEFE (Jiangsu, China) and are listed in Table 1. All primer sequences were verified against the rat genome assembly and validated by sequencing of PCR products. Only a single amplicon of the expected size was detected for each gene. The qPCR amplification protocol was as follows: initial denaturation at 95 °C for 15 min, followed by 40 cycles of 95 °C for 10 s, 60 °C for 20 s, and 72 °C for 30 s. Melt-

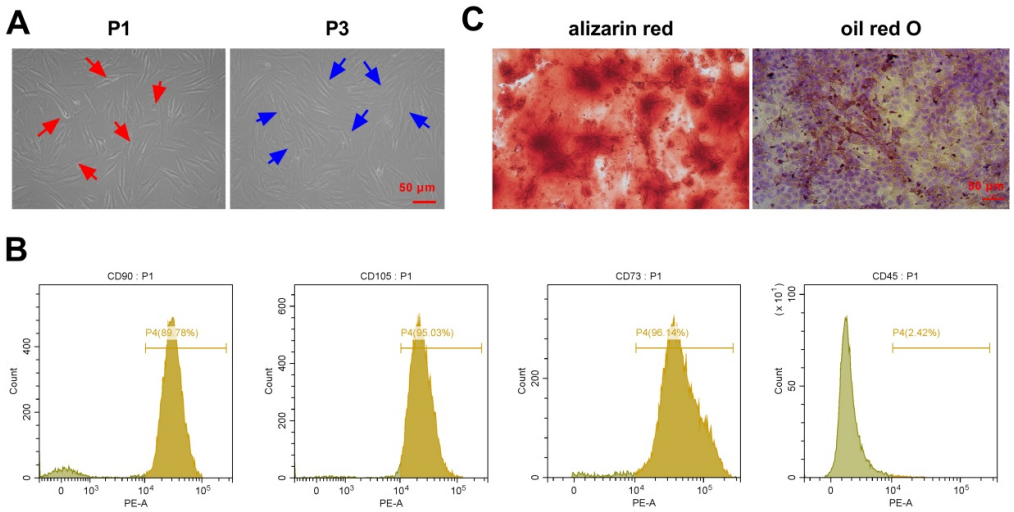

Fig. 1. Isolation and identification of BMSCs. (**A**) The morphology of the BMSCs at P1 and P3 was observed. Scale bar: 50 μm. Red arrows: mixed spindle-shaped and polygonal cells. Blue arrows: uniform spindle-shaped cells. (**B**) Analysis of CD90, CD105, CD73, and CD45 expression on BMSCs at P3 using flow cytometry. (**C**) Alizarin red and oil red O staining were conducted to evaluate the osteogenic and adipogenic differentiation of BMSCs at P3. Scale bar: 100 μm.

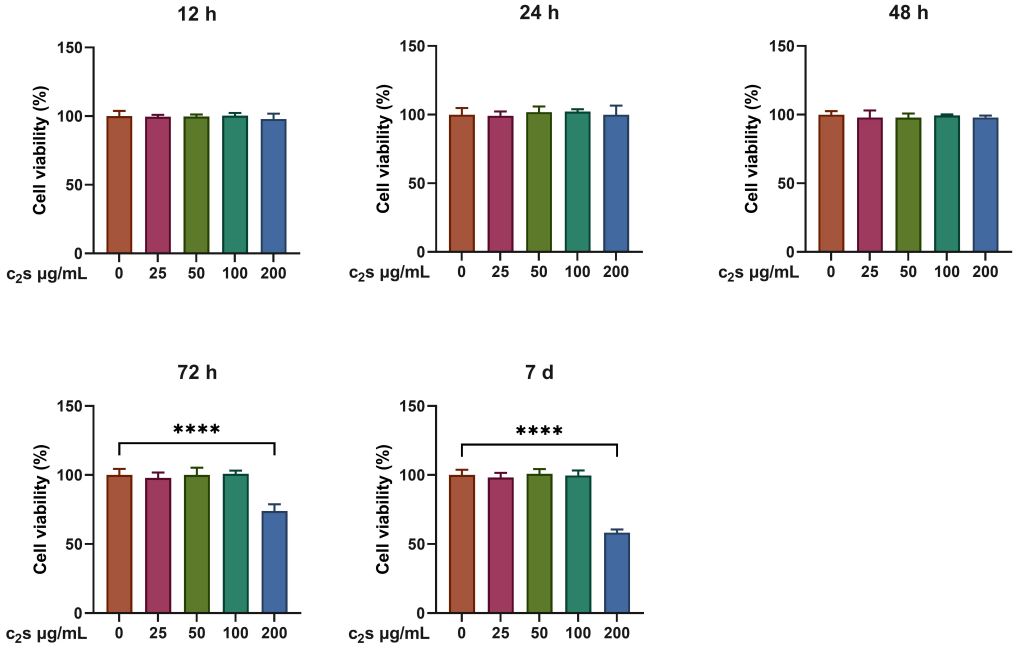

Fig. 2. Proliferative effect of C_2S on BMSCs. The BMSCs were exposed to 0, 25, 50, 100, or 200 μg/mL C_2S for 12, 24, 48, 72 h, or 7 d. A CCK-8 assay was performed to evaluate the cytotoxicity of C_2S to the BMSCs. The data are expressed as the means ± SDs (n = 3). $^{****}p < 0.0001$ vs. the 0 μg/mL C_2S group.

ing curve analysis was performed at the end of each run to ensure amplification specificity. Relative quantification of *β-catenin*, Runt-related transcription factor 2 (*Runx2*), osteopontin (*OPN*), and osteocalcin (*OCN*) transcripts was performed via the $2^{-\Delta\Delta Ct}$ method, with glyceraldehyde-3-phosphate dehydrogenase (*GAPDH*) used as a reference gene. *GAPDH* is one of the most stably expressed and widely used reference genes in BMSC osteogenic differentiation studies, as supported by previous publications in the field [20–22].

Western Blot Analysis

Following the indicated treatments, BMSCs were cultured for 14 days for osteogenic induction. After that,

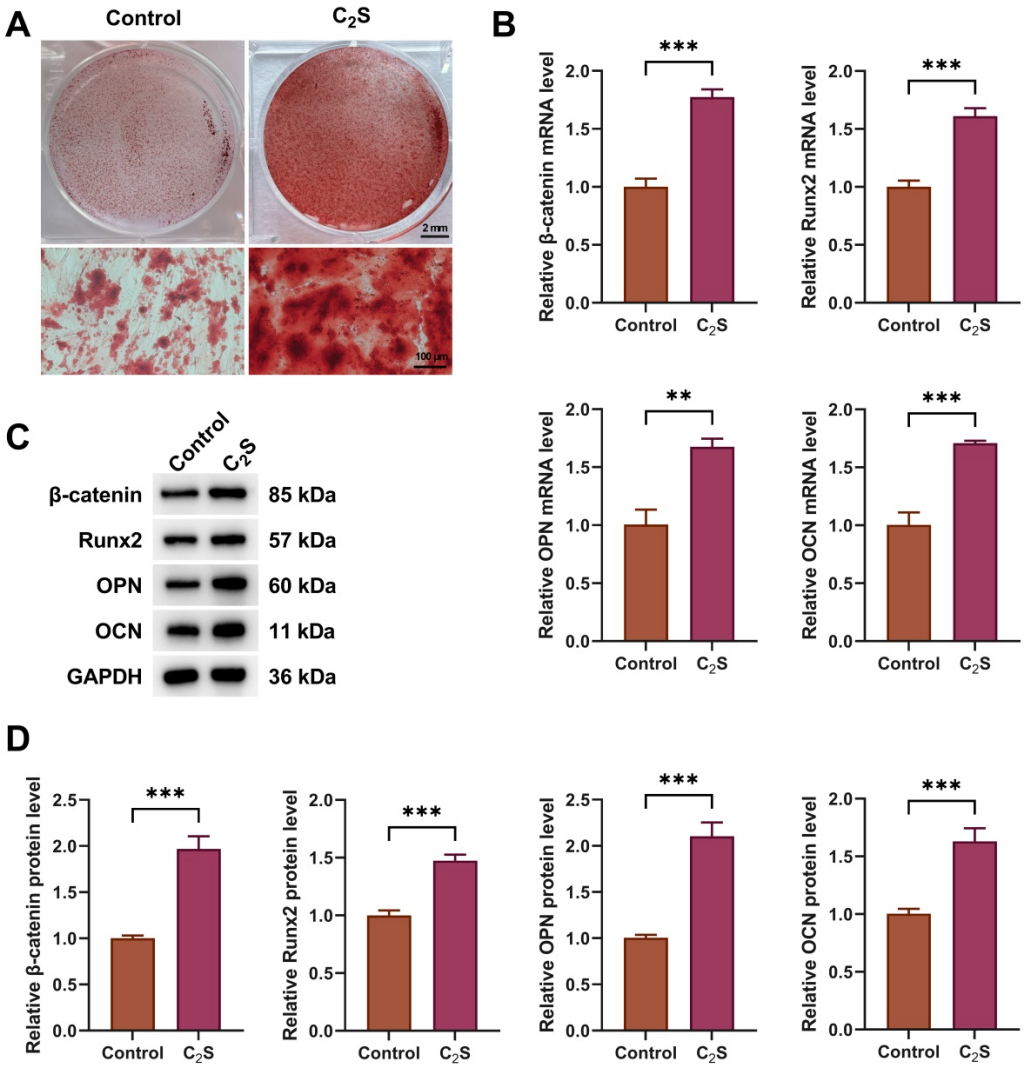

Fig. 3. C_2S facilitated osteogenic differentiation of BMSCs. BMSCs were cultured in OIM and treated with or without 100 μg/mL C_2S for 7 d or 14 d. (**A**) Alizarin red staining was performed to assess mineralized nodules at 14 d after C_2S exposure. (**B,C**) qRT-PCR (**B**) and Western blotting (**C**) were conducted to analyze the mRNA and protein levels of *β-catenin*, *Runx2*, *OPN*, and *OCN* at 7 d after C_2S exposure. (**D**) Quantification of the protein levels of *β-catenin*, *Runx2*, *OPN*, and *OCN* in (**C**). The data are expressed as the means ± SDs (n = 3). $^{**}p < 0.01$, $^{***}p < 0.001$ vs. the control group.

the cells were harvested and protein extracts were obtained with Western/IP cell lysis buffer (P0013, Beyotime, Shanghai, China), after which the protein concentration was measured by a bicinchoninic acid (BCA) assay (P0010, Beyotime, Shanghai, China). After separation via sodium dodecyl dulfate-polyacrylamide gel electrophoresis (SDS-PAGE) (G2003, Servicebio, Wuhan, China) and electrotransfer to polyvinylidene fluoride (PVDF) membranes (FFP22, Beyotime, Shanghai, China), nonspecific binding sites were blocked with 5 % nonfat-dried for 60 min. The membranes were probed with primary antibodies, including anti-*β-catenin* (1:1000, ER0805, HuaBio, Hangzhou, China), anti-*OCN* (1:1000, ER1919-20, HuaBio, Hangzhou, China), anti-*Runx2* (1:500, 20700-1-AP, Proteintech, Wuhan, China), anti-*OPN* (1:1000, 83413-6-RR, Proteintech, Wuhan, China), and anti-*GAPDH* (1:5000, 60004-1-Ig, Proteintech, Wuhan, China), at 4 °C overnight. The membranes were incubated with secondary antibodies (1:2000, ZB-2305, ZB-2301, ZSGB-BIO, Beijing, China) at 37 °C for 1 h prior to development with Immobilon Western HRP Substrate Luminol Reagent (WBKLS0050, Merck Millipore, Billerica, MA, USA) and observed on a Luminescent Imaging System (Tanon-4600, Yuanpinghao Biotechnology, Beijing, China).

Animals

Ten four-week-old (120 ± 10 g) and 30 twelve-week-old (320 ± 10 g) Sprague-Dawley female rats were supplied by Experimental Animal Center of Zhengzhou University (Zhengzhou, China). The rats were kept under spe-

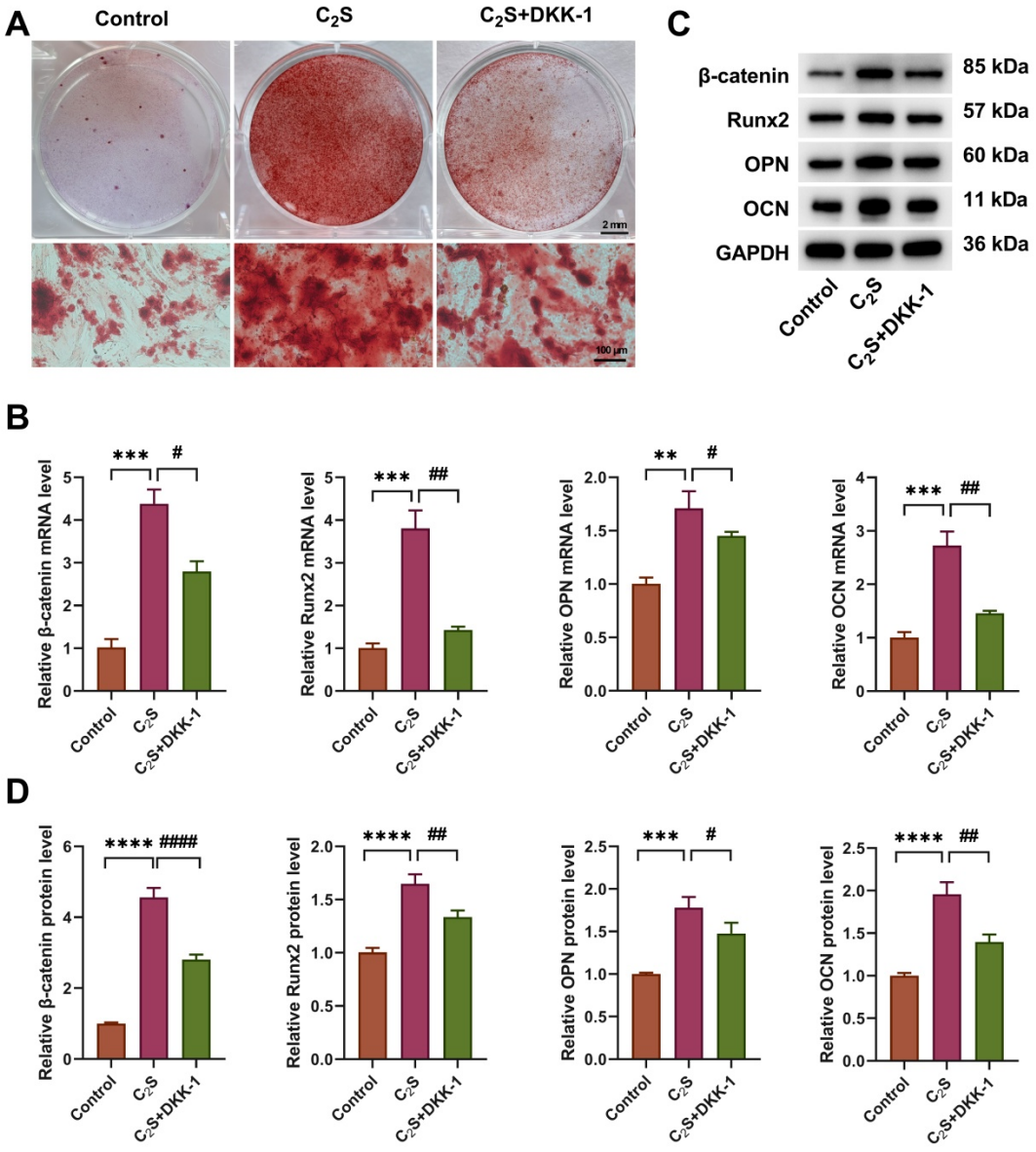

Fig. 4. C_2S promoted osteogenic differentiation of BMSCs by activating the Wnt/*β-catenin* signaling pathway. BMSCs were cultured in OIM and incubated with 0.5 μg/mL Wnt inhibitor (DKK-1) for 1 h, followed by treatment with or without 100 g/mL C_2S for 7 d or 14 d. (**A**) Alizarin red staining was performed to assess mineralized nodules at 14 d after C_2S exposure. (**B,C**) qRT-PCR (**B**) and Western blotting (**C**) were conducted to analyze the mRNA and protein levels of *β-catenin*, *Runx2*, *OPN*, and *OCN* at 7 d after C_2S exposure. (**D**) Quantification of the protein levels of *β-catenin*, *Runx2*, *OPN*, and *OCN* in (**C**). The data are expressed as the means ± SDs (n = 3). $^{**}p < 0.01$, $^{***}p < 0.001$, $^{****}p < 0.0001$ vs. the control group; $\#p < 0.05$, $\#\#p < 0.01$, $\#\#\#\#p < 0.0001$ vs. the C_2S group.

cific pathogen-free conditions (22 ± 2 °C, 55 %–70 % humidity) with a 12-h light/dark cycle. Food and water were provided ad libitum.

Animal Grouping and Treatments

As previously described [27], 30 twelve-week-old rats were acclimated for one week and then subjected to ovariectomy to establish an osteoporosis model after being anesthetized by intraperitoneal injection of 1 % pentobarbital sodium (40 mg/kg). Upon successful preparation of the osteoporosis model, distal femoral bone defects were generated in the remaining 24 rats as previously described [28]. In brief, an incision was made on the outer side of the thigh following anesthesia of the rats. During the procedure, an incision was created parallel to the femur, separating the subcutaneous and muscle tissues to uncover the outer femoral condyle. A dental implant machine (112032, Jinme, Guangzhou, China) equipped with a 3 mm diame-

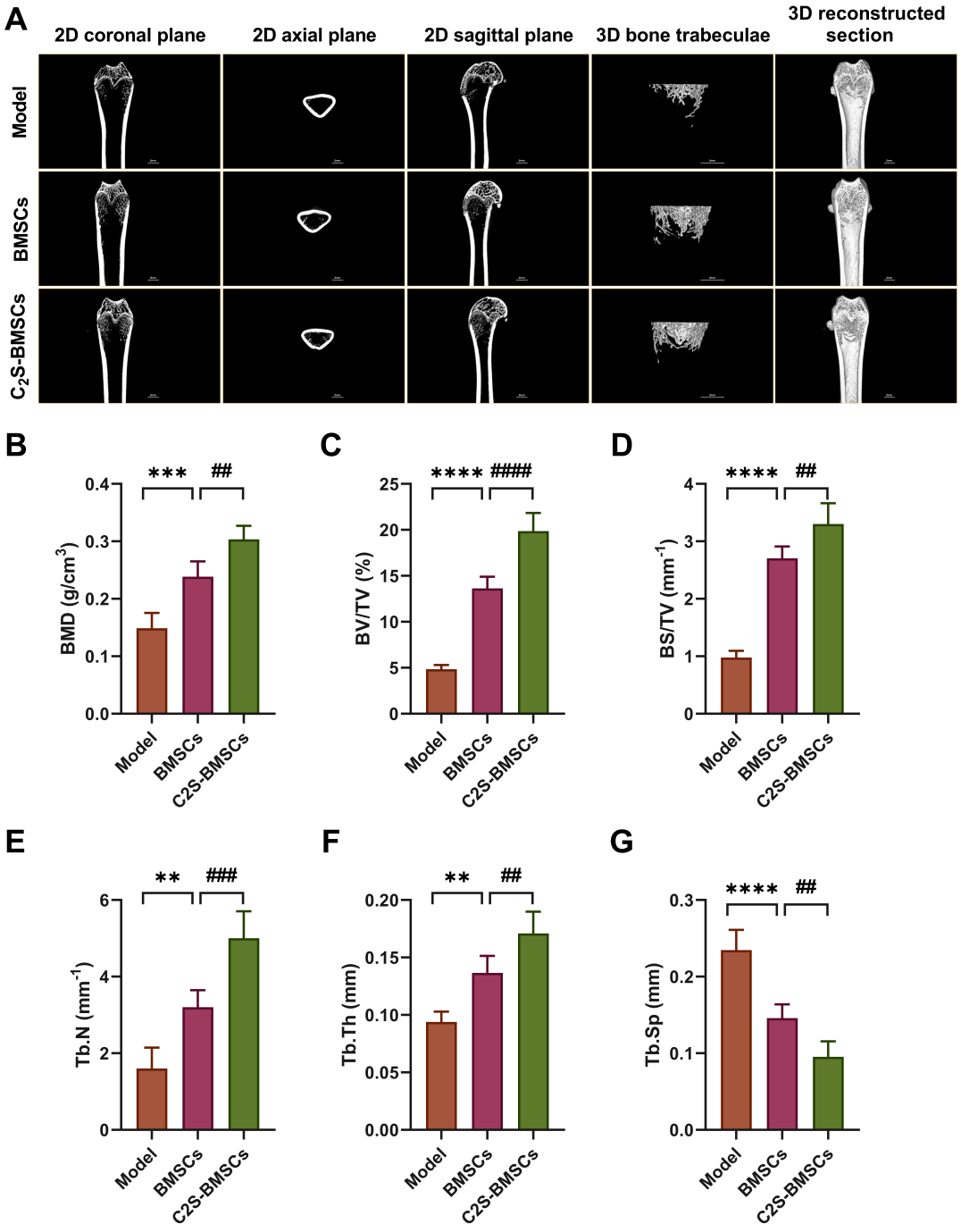

Fig. 5. Micro-CT analysis of bone repair in femur defects of osteoporotic rats. Femoral defects were surgically induced in osteoporotic rats at 3 months following ovariectomy, with subsequent implantation of BMSC or C_2S-BMSC scaffolds. Defects without intervention served as the model control. (**A**) Representative 2D and 3D micro-CT images of the femoral defect sites 8 weeks post-implantation. (**B–G**) Quantitative analyses of BMD (**B**), BV/TV (**C**), BS/TV (**D**), Tb.N (**E**), Tb.Th (**F**), Tb.Sp. (**G**) in the defect area. The data are expressed as the means ± SDs (n = 8). $^{**}p < 0.01$, $^{***}p < 0.001$, $^{****}p < 0.0001$ vs. the model group; $\#\#p < 0.01$, $\#\#\#p < 0.001$, $\#\#\#\#p < 0.0001$ vs. the BMSC group.

ter drill bit operating at 40,000 rpm was used to drill from the outer surface to the inner side until the opposite cortical bone was reached, with an approximate depth of 4 mm. The samples were rinsed with normal saline until no noticeable bone debris remained. Subsequently, the rats were randomized into 3 groups with a random number generator: model, BMSC, and C_2S-BMSC groups. The experimental unit was the individual rats (n = 8 per group).

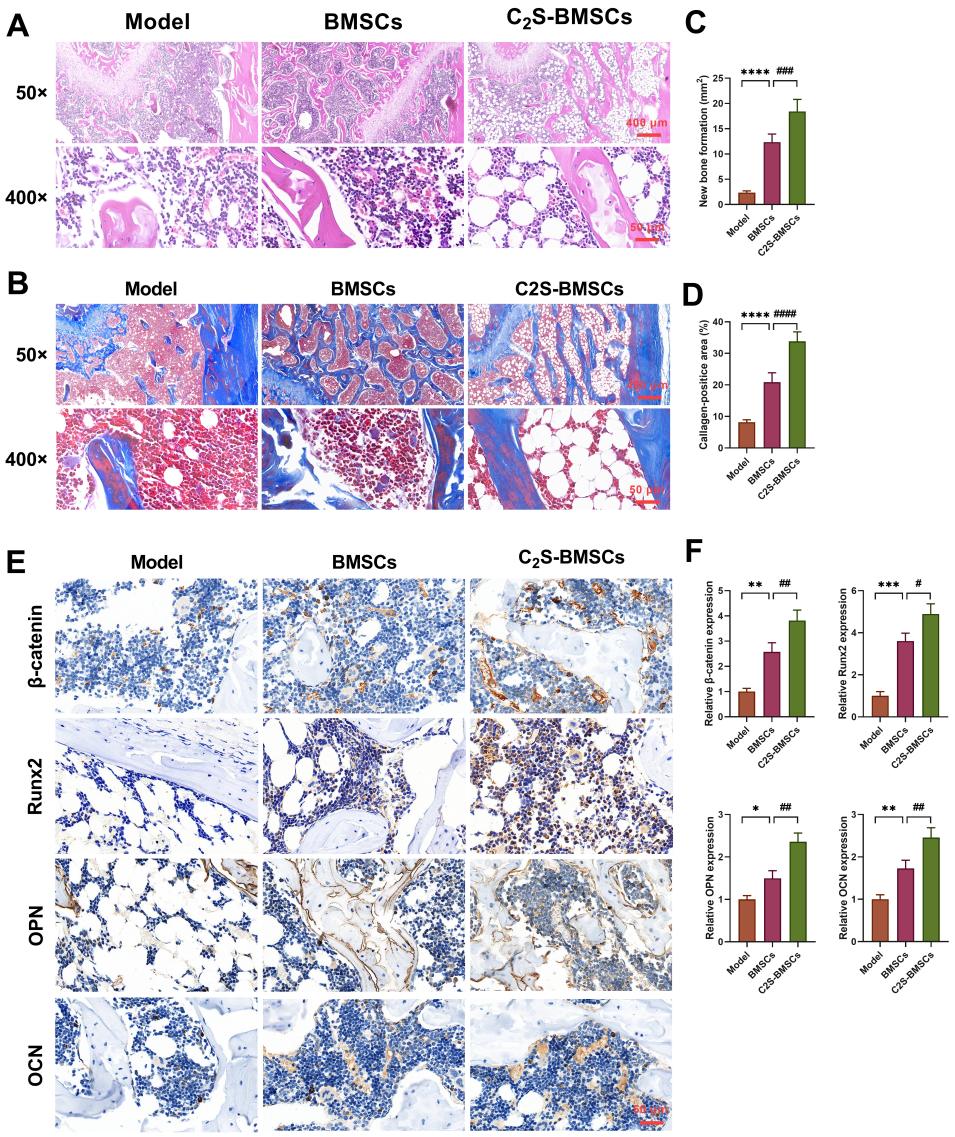

Fig. 6. Histological examination of regenerated bone tissue in osteoporotic rat femoral defects. (**A**) The defect area was histologically evaluated through HE staining. Scale bars: 400 μm and 50 μm. (**B**) The formation of new bone and fibers was assessed via Masson's trichrome staining. Scale bars: 400 μm and 50 μm. Quantitative analysis of the new bone formation area (**C**) according to HE staining and the collagen-positive area (**D**) according to Masson's trichrome staining. (**E**) IHC was performed to examine the expressions of *β-catenin*, *Runx2*, *OPN*, and *OCN*. Scar bar: 50 μm. (**F**) The expression of *β-catenin*, *Runx2*, *OPN*, and *OCN* was quantified in (**E**). The data are expressed as the means ± SDs (n = 8). $^{*}p < 0.05$, $^{**}p < 0.01$, $^{***}p < 0.001$, $^{****}p < 0.0001$ vs. the model group; $\#p < 0.05$, $\#\#p < 0.01$, $\#\#\#p < 0.001$, $\#\#\#\#p < 0.0001$ vs. the BMSC group.

The model group served as the internal control to simulate the natural progression of osteoporotic bone defects without intervention. The BMSC and C_2S-BMSC groups were compared against this baseline to evaluate their therapeutic efficacy. The rats in the model group were given only collagen-based scaffolds at the femoral defect site, whereas the BMSC and C_2S-BMSC groups received the BMSC and C_2S-BMSC scaffolds, respectively. Once the scaffolds were implanted, the periosteum and skin were stitched. Post-surgery, 80,000 units of penicillin were administered intramuscularly to each rat daily for three days to prevent infection. Eight weeks after the operation, the animals were humanely sacrificed by intraperitoneal injection of 150 mg/kg 1 % pentobarbital sodium. The model group served as the internal control to simulate the natural progression of osteoporotic bone defects without intervention. Investigators performing surgeries and behavioral tests were blinded to group allocation. The statistician was unblinded during analysis.

Micro-computed tomography (CT)

After 24 h of fixation in 4 % paraformaldehyde, the femurs were scanned by micro-CT (NMC-200, PINGSENG SCIENTIFIC, Kunshan, China). A length of 7 mm from the distal end of the femur was chosen for scanning, with parameters set at the radial field of view: 100 mm, maximum axial scanning range: 250 mm, fastest scanning: 4 s/bed, and reconstructed pixel size: Min. 2 μm. Following scanning, the images were examined. The region of interest for the femur was a 3 $\times$ 2.5 mm cylinder within the defect area. The BMD, bone volume fraction (BV/TV), bone surface density (BS/TV), trabecular bone quantity (Tb.N), trabecular bone thickness (Tb.Th), and trabecular separation (Tb.Sp) were measured and calculated.

Regular and Special Staining

After the microtomographic analysis, femur samples were prepared for histological analysis using hematoxylin and eosin (HE) (C0105S, Beyotime, Shanghai, China) and Masson trichrome (C0189S, Beyotime, Shanghai, China) staining kits according to the manufacturer's protocol. Briefly, after 7 days of fixation with 4 % paraformaldehyde and 4 weeks of decalcification with 10 % ethylenediaminetetraacetic acid (EDTA), the femurs were placed in paraffin, and sections (4 μm thick) were obtained from the central region of the defect. For HE staining, after dewaxing and rehydration, the sections were stained with hematoxylin for 10 min at room temperature, followed by eosin staining for 2 min. For Masson trichrome staining, the sections were stained with Weigert's iron hematoxylin for 10 min, phosphomolybdic acid for 10 min, and aniline blue for 5 min in sequence. The microscopic examination was performed on a microscope (CK31, Olympus, Tokyo, Japan). New bone formation and the area of collagen deposition were quantified via HE and Masson's trichrome staining, respectively [29,30].

Immunohistochemical (IHC) Staining

After dewaxing and rehydration, the paraffin sections of the femur were immersed in EDTA antigen retrieval solutions at 100 °C for 20 min for antigen retrieval. The slides were then incubated in 3 % H_2O_2 for 20 min at room temperature and blocked with 5 % bovine serum albumin (SW3015, Solarbio, Beijing, China) for 30 min. The primary antibodies against *β-catenin* (1:500, ER0805, HuaBio, Hangzhou, China), *Runx2* (1:200, 20700-1-AP), *OPN*(1:500, ER1919-20) and *OCN* (1:500, 83413-6-RR) were applied to incubate the sections at 4 °C overnight. The sections were incubated with HRP-conjugated secondary antibodies (GB23303, GB23301, Servicebio, Wuhan, China) for 1 h at room temperature. Signals were developed using 3,3'-diaminobenzidine (DAB) substrate (PA140212, TIANGEN, Beijing, China) for 3 min. Nuclei were counterstained with hematoxylin (AR1108, BOSTER, Wuhan, China), the slides were dehydrated, cleared in xylene, and mounted with neutral resin. The sections were imaged under a light microscope (CK31, Olympus, Tokyo, Japan). Semi-quantitative analysis was performed using a whole slide scanner (Pannoramic SCAN, 3D Histech, Budapest, Hungary) by measuring integrated optical density in five random fields per sample.

Statistical Analysis

The results are presented as the means $\pm$ standard deviations (SDs) from three independent experiments (*in vitro* experiments), and the *in vivo* data are presented as the means $\pm$ SDs (n = 8 per group). Data analysis was conducted with GraphPad Prism 9.5.0 (GraphPad Software, Inc., San Diego, CA, USA). The Student's *t*-test was used to assess differences between two groups, whereas one-way ANOVA followed by Tukey's post hoc test was used to compare multiple groups. Statistical significance was indicated by $p < 0.05$.

Results

BMSCs were Successfully Isolated and Identified from Rats

After the rats were sacrificed, BMSCs were collected from their femurs and cultured for morphological examination. The cells in the first passage (P1) were fusiform and polygonal, whereas the P3 cells were uniformly fusiform (Fig. 1**A**). Flow cytometry revealed that CD90, CD105, and CD73 were present on nearly all P3 cells, whereas CD45 was almost not expressed on the surface of the P3 cells (Fig. 1**B**). Additionally, P3 BMSCs efficiently differentiated into osteoblasts and adipocytes in OIM and AIM (Fig. 1**C**). Therefore, BMSCs were successfully isolated and identified from rats.

Proliferative Effect of C_2S on BMSCs

BMSCs exposure to C_2S (25, 50, or 100 μg/mL) for 12, 24, 48, or 72 h or 7 d had no notable effect on cell proliferation ($p > 0.05$). However, exposure of the BMSCs to 200 μg/mL C_2S resulted in a significant decrease in cell viability ($p < 0.0001$, Fig. 2). Consequently, 100 μg/mL C_2S was used for the subsequent experiments.

C_2S Facilitated Osteogenic Differentiation of BMSCs

Alizarin red staining revealed notably mineralized nodules at 14 days after osteogenic differentiation (Fig. 3**A**). Compared with the control, C_2S notably increased the messenger ribonucleic acid (mRNA) ($p < 0.001$, Fig. 3**B**) and protein ($p < 0.001$, Fig. 3**C,D**) expression levels of osteogenesis-associated molecules, such as *β-catenin*, *Runx2*, *OPN*, and *OCN*. This evidence suggested that C_2S might support the osteogenesis of BMSCs.

C_2S Promoted BMSC Osteogenic Differentiation by Activating the Wnt/β-catenin Signaling Pathway

The Wnt/*β-catenin* signaling pathway influences the fate of BMSCs, directing them to differentiate into osteoblasts [10]. Thus, BMSCs were treated with 0.5 μg/mL DKK-1 for 1 h before being exposed to 100 μg/mL C_2S. The presence of mineralized nodules in BMSCs was prominently induced by C_2S, but DKK-1 notably diminished these nodules, as determined by Alizarin red staining (Fig. 4**A**). qPCR and Western blot analyses were employed to evaluate the mRNA and protein expression of osteoblast-associated genes in BMSCs. C_2S caused considerable increases in the mRNA and protein expression levels of *β-catenin*, *Runx2*, *OPN*, and *OCN* compared with those in the control group ($p < 0.001$), and these increases were notably blocked by DKK-1 ($p < 0.01$, Fig. 4**B–D**). These results led us to conclude that C_2S promoted the osteogenic differentiation of BMSCs via Wnt/*β-catenin* pathway activation.

C_2S Promoted Bone Defect Repair by Inducing BMSC Osteogenic Differentiation in Osteoporotic Rats

To first validate the successful establishment of the osteoporotic bone defect model, we analyzed the outcomes in the untreated Model group. Micro-CT analysis at the endpoint revealed minimal bone regeneration within the femoral defect site (Fig. 5**A**, Model group), confirming the creation of a persistent, critical-sized defect. Furthermore, the bone microstructure in the Model group exhibited a severely osteoporotic phenotype, characterized by significantly lower values for BMD, BV/TV, BS/TV, Tb. N, and Tb. Th, alongside higher Tb. Sp (Fig. 5**B–G**). Histological findings corroborated this, showing that the defect areas in the Model group were predominantly filled with fibrous connective tissue with only sporadic new bone formation (Fig. 6**A,B**, Model group). These data collectively confirm the robustness of our osteoporotic bone defect model.

Having established this pathological baseline, we next evaluated the therapeutic efficacy of the implants. The two dimensional (2D) and 3D micro-CT images revealed substantially greater bone formation areas in the BMSC group than in the model group and further augmented regenerative outcomes in the C_2S-BMSC group compared with the BMSCs group (Fig. 5**A**). Compared with the model group, the BMSC group presented markedly greater BMD, BV/TV, BS/TV, Tb.N, and Tb.Th values but lower Tb.Sp values ($p < 0.01$). Notably, compared with the BMSC group, the C_2S-BMSC group presented superior outcomes, with much greater differences in BMD, BV/TV, BS/TV, Tb.N, and Tb.Th and further reductions in Tb.Sp ($p < 0.01$, Fig. 5**B–G**). Histological staining revealed that the defect areas contained predominantly fibrous connective tissue with only sporadic new bone formation in the model group. In contrast, BMSC and C_2S-BMSC scaffold implantation markedly enhanced osseous regeneration in osteoporotic rats, as demonstrated by the presence of multiple well-defined ossification foci, densely organized trabecular networks, and abundant vasculature, indicating robust bone repair activity and the accumulation of collagen formation and bone mineralization (Fig. 6**A,B**). Furthermore, qualitative analysis revealed that, compared with those in the BMSC group, more new bone formation and collagen accumulation were produced in the C_2S-BMSC group ($p < 0.001$, Fig. 6**C,D**). IHC results showed that BMSC resulted in significant upregulation of *β-catenin*, *Runx2*, *OPN*, and *OCN* compared with the model group, and further enhancement of *β-catenin*, *Runx2*, *OPN*, and *OCN* was found in the C_2S-BMSC group than those in the BMSC group ($p < 0.05$, Fig. 6**E,F**). The results strongly suggested that C_2S enhanced bone regeneration in osteoporotic rats by activating BMSC osteogenic differentiation.

Discussion

Bone defect regeneration involves diverse biological mechanisms and intricate signaling pathways [31]. Osteoporosis occurs when there is a disruption in the equilibrium between bone resorption and bone formation, where bone breakdown outpaces new bone formation, while the regenerative capacity is compromised. As a result, therapeutic interventions for osteoporotic bone defects present greater challenges than do nonosteoporotic bone defects in the clinic [32]. Nevertheless, existing therapeutic options show restricted effectiveness and often yield unsatisfactory outcomes. This highlights the demand for new pharmacological interventions that are not only potent and safe but also widely accessible to address osteoporosis and its complications.

Bone tissue engineering utilizing cellular therapy represents an advanced strategy for repairing bone defects [33,34]. BMSCs, in particular, have gained significant attention in bone regeneration research owing to their broad range of tissue sources, robust proliferation ability, and capacity to undergo osteogenic differentiation under appropriate conditions. These properties make them a preferred choice for tissue engineering applications [35]. Notably, combining BMSCs with bioscaffolds demonstrates superior efficacy relative to cell-free scaffold approaches [36,37]. C_2S, a key constituent of bioactive glasses, is an amorphous silicate-based material with excellent biocompatibility and osteoconductive properties, enabling direct chemical bonding with bone tissue. Owing to these characteristics, it is widely utilized in bone graft substitutes and synthetic bone powders and is a favorable option for dental and orthopedic implant applications [38–40]. The present study confirmed that C_2S (0–100 μg/mL) had no cytotoxic effects on BMSC viability, supporting its biocompatibility with osteoprogenitor cells and aligning with earlier published findings [20]. C_2S coating-derived ionic products partially induced BMSC osteogenesis by increasing osteoblastic gene expression (*Runx2* and *OCN*) and mineralization capacity [23]. C_2S triggers macrophagic inflammation via mi-

tochondrial dysfunction and autophagy, subsequently enhancing the osteogenic capacity of BMSCs [25]. By activating mTOR/ULK1-dependent autophagy, C_2S nanoparticles activate the Wnt/*β-catenin* signaling pathway, thereby enhancing BMSC bone-formation ability and bone matrix mineralization by upregulating *β-catenin*, BMP2, *Runx2*, *OPN*, and Axin1 levels [20]. In agreement with the aforementioned findings, the bone-promoting effects of C_2S were validated by increased mineralization capacity and increased levels of bone formation regulators (*β-catenin*, *Runx2*) and bone matrix proteins (*OPN*, *OCN*) in C_2S-treated BMSCs compared with those in control cells in our present study. According to these findings, C_2S induced BMSC osteogenesis *in vitro*. Through a murine skull defect model, Ruolan *et al*. [20] revealed that C_2S nanoparticle implantation promoted greater new bone formation and higher BV/TV values relative to control groups. In addition, Zhong *et al*. [22] reported that C_2S significantly enhanced cranial defect healing in rats, along with increasing BV/TV and BS/TV ratios; histological assessment revealed organized new bone formation extending from defect margins to central regions and superior collagen maturation in rats treated with C_2S. Our present research utilized a rat model with osteoporotic femoral defects to investigate the therapeutic potential of C_2S in bone regeneration. Micro-CT and histological analyses revealed that, compared with the model treatment, both the C_2S and C_2S-BMSC treatments markedly enhanced bone regeneration and improved the trabecular microstructure in the defect area. Substantial increases in the BMD, BV/TV, BS/TV, Tb.N, and Tb.Th were observed, accompanied by a notable reduction in the Tb.Sp. Compared with BMSCs alone, the C_2S-BMSC composite demonstrated superior regenerative efficacy, suggesting that C_2S may facilitate bone healing through BMSC-mediated osteogenesis in osteoporotic bone defects *in vivo*.

The Wnt signaling cascade serves as a master regulator of osteogenic differentiation, directly modulating BMSC fate commitment through *β-catenin*-dependent transcriptional activation of osteogenic programs [41]. Pharmacological activation of Wnt signaling represents a promising therapeutic strategy to enhance BMSC osteogenic differentiation for bone regeneration applications [42]. Canonical Wnt signaling directs MSC lineage commitment through *β-catenin*-dependent mechanisms. *β-catenin* nuclear accumulation promotes osteogenesis via the formation of *β-catenin*/T-cell factor (TCF)/lymphoid enhancer-binding factor (LEF) transcriptional complexes to upregulate specificity protein 7 (Sp7) and *Runx2* expression, whereas *β-catenin* deficiency shifts differentiation toward adipogenesis through PPARγ/CCAAT/enhancer-binding protein alpha (C/EBPα) activation [43,44]. Activation of the Wnt/*β-catenin* signaling pathway cascade effectively mitigates bone loss in ovariectomized mice [45]. Recent evidence confirms that multiple therapeutic agents, including pharmaceuticals, bioactive molecules, extracellular vesicles, and engineered biomaterials, have been identified as potent Wnt/*β-catenin* activators that enhance the osteogenic differentiation of BMSCs in osteoporotic conditions [42]. Ruolan *et al*. [20] demonstrated that C_2S nanoparticles undergo nuclear translocation, where they directly interact with *β-catenin* to increase its transcriptional activity, thereby promoting osteogenic differentiation in BMSCs. In this study, DKK-1 pretreatment effectively suppressed C_2S-induced osteogenic differentiation in BMSCs, as evidenced by a reduction in mineralized nodule formation and the downregulation of *β-catenin*, *Runx2*, *OPN*, and *OCN*, confirming the essential function of Wnt/*β-catenin* signaling in the differentiation of BMSCs triggered by C_2S.

While the current findings show encouraging outcomes, certain limitations should be acknowledged. First, this study evaluated only short-term effects (an 8-week period), while extended observation is needed to determine long-term bone remodeling and biomechanical stability. Second, since rodent-derived BMSCs may not entirely replicate human cellular behavior, future studies should incorporate human cell-based or preclinical models for validation. Third, the lack of *in vivo* mechanistic investigations using pathway inhibitors limits the conclusive interpretation of the signaling mechanisms involved. Fourth, the precise pathway by which C_2S modulates Wnt signaling, whether through direct receptor binding or secondary regulation of extracellular mediators (e.g., sclerostin), remains to be elucidated. Fifth, the absence of healthy/non-osteoporotic controls prevents direct comparison of model induction efficacy. Finally, comprehensive biocompatibility testing was not performed due to resource constraints. However, these aspects were considered secondary to the primary goal of evaluating therapeutic efficacy in an established model system. Further studies will be performed to address these limitations.

Conclusions

In summary, the present study demonstrated that C_2S promoted BMSC bone-promoting capability via Wnt/*β-catenin* signaling pathway activation and increased bone regeneration in osteoporotic rats. These findings position C_2S as an encouraging biomaterial for constructing bone tissue, particularly in osteoporosis-related defects. Future research should address translational challenges and refine the mechanistic understanding to facilitate clinical adoption.

List of Abbreviations

α-MEM, alpha-minimum essential medium; AIM, adipogenic induction medium; BMD, bone mineral density; BMSCs, bone marrow mesenchymal stem cells; BS/TV, bone surface density; BV/TV, bone volume fraction; CCK-8, cell counting kit-8; C_2S, dicalcium silicate; DKK-1, Dickkopf-1; FBS, fetal bovine serum; *GAPDH*, glyceraldehyde-3-phosphate dehydrogenase; HE, hema-

toxylin and eosin; *OCN*, osteocalcin; OIM, osteogenic induction medium; *OPN*, osteopontin; P1, first passage; P3, third-passage; qRT-PCR, quantitative real-time PCR; *Runx2*, Runt-related transcription factor 2; Tb.N, trabecular bone quantity; Tb.Sp, trabecular separation; Tb.Th, trabecular bone thickness; SDs, standard deviations; IHC, immunohistochemical; PCR, polymerase chain reaction; mRNA, messenger ribonucleic acid; CT, computed tomography; PPARγ, peroxisome proliferator-activated receptor gamma; PBS, phosphate-buffered saline; IgG, immunoglobulin G; cDNA, complementary deoxyribonucleic acid; qPCR, quantitative polymerase chain reaction; BCA, bicinchoninic acid; SDS-PAGE, sodium dodecyl dulfate-polyacrylamide gel electrophoresis; PVDF, polyvinylidene fluoride; EDTA, ethylenediaminetetraacetic acid; DAB, 3,3'-diaminobenzidine; 2D, two dimensional; TCF, T-cell factor; LEF, lymphoid enhancer-binding factor; Sp7, specificity protein 7; C/EBPα, CCAAT/enhancer-binding protein alpha.

Availability of Data and Materials

The datasets used and/or analyzed during the current study are available from the corresponding author on reasonable request.

Author Contributions

XZ designed the research study. XZ and QZ performed the research. BYZ provided help and advice on data interpretation. BYZ and RL analyzed the data. XZ wrote the manuscript. All authors contributed to editorial changes in the manuscript. All authors read and approved the final manuscript.

Ethics Approval and Consent to Participate

The Scientific Research and Clinical Trial Ethics Committee of the First Affiliated Hospital of Zhengzhou University (Zhengzhou, China) approved all the experiments (Approval No. 2025-KY-0859), ensuring they complied with the ARRIVE guidelines for conducting animal research.

Acknowledgments

Not applicable.

Funding

Not applicable.

Conflict of Interest

The authors declare no conflict of interest.

References

[1] Muñoz M, Robinson K, Shibli-Rahhal A. Bone Health and Osteoporosis Prevention and Treatment. Clinical Obstetrics and Gynecology. 2020; 63: 770–787. https://doi.org/10.1097/grf.0000000000000572.

[2] Föger-Samwald U, Dovjak P, Azizi-Semrad U, Kerschan-Schindl K, Pietschmann P. Osteoporosis: Pathophysiology and therapeutic options. EXCLI Journal. 2020; 19: 1017–1037. https://doi.org/10.17179/excli2020-2591.

[3] Salari N, Ghasemi H, Mohammadi L, Behzadi MH, Rabieenia E, Shohaimi S, *et al*. The global prevalence of osteoporosis in the world: a comprehensive systematic review and meta-analysis. Journal of Orthopaedic Surgery and Research. 2021; 16: 609. https://doi.org/10.1186/s13018-021-02772-0.

[4] Baek YH, Cho SW, Jeong HE, Kim JH, Hwang Y, Lange JL, *et al*. 10-Year Fracture Risk in Postmenopausal Women with Osteopenia and Osteoporosis in South Korea. Endocrinology and Metabolism. 2021; 36: 1178–1188. https://doi.org/10.3803/EnM.2021.1215.

[5] Stanovici J, Le Nail LR, Brennan MA, Vidal L, Trichet V, Rosset P, *et al*. Bone regeneration strategies with bone marrow stromal cells in orthopaedic surgery. Current Research in Translational Medicine. 2016; 64: 83–90. https://doi.org/10.1016/j.retram.2016.04.006.

[6] Khosla S, Hofbauer LC. Osteoporosis treatment: recent developments and ongoing challenges. The Lancet. Diabetes & Endocrinology. 2017; 5: 898–907. https://doi.org/10.1016/s2213-8587(17)30188-2.

[7] Marie PJ, Fromigué O. Osteogenic differentiation of human marrow-derived mesenchymal stem cells. Regenerative Medicine. 2006; 1: 539–548. https://doi.org/10.2217/17460751.1.4.539.

[8] Jiang Y, Zhang P, Zhang X, Lv L, Zhou Y. Advances in mesenchymal stem cell transplantation for the treatment of osteoporosis. Cell Proliferation. 2021; 54: e12956. https://doi.org/10.1111/cpr.12956.

[9] Amarasekara DS, Kim S, Rho J. Regulation of Osteoblast Differentiation by Cytokine Networks. International Journal of Molecular Sciences. 2021; 22: 2851. https://doi.org/10.3390/ijms22062851.

[10] Visweswaran M, Pohl S, Arfuso F, Newsholme P, Dilley R, Pervaiz S, *et al*. Multi-lineage differentiation of mesenchymal stem cells-To Wnt, or not Wnt. The International Journal of Biochemistry & Cell Biology. 2015; 68: 139–147. https://doi.org/10.1016/j.biocel.2015.09.008.

[11] Baron R, Kneissel M. WNT signaling in bone homeostasis and disease: from human mutations to treatments. Nature Medicine. 2013; 19: 179–192. https://doi.org/10.1038/nm.3074.

[12] Marini F, Giusti F, Palmini, G, Brandi, ML. Role of Wnt signaling and sclerostin in bone and as therapeutic targets in skeletal disorders. Osteoporosis International: a Journal Established as Result of Cooperation between the European Foundation for Osteoporosis and the National Osteoporosis Foundation of the USA. 2023; 34: 213–238. https://doi.org/10.1007/s00198-022-06523-7.

[13] Hu L, Chen W, Qian A, Li YP. Wnt/β-catenin signaling components and mechanisms in bone formation, homeostasis, and disease. Bone Research. 2024; 12: 39. https://doi.org/10.1038/s41413-024-00342-8.

[14] Gao Y, Chen N, Fu Z, Zhang Q. Progress of Wnt Signaling Pathway in Osteoporosis. Biomolecules. 2023; 13: 483. https://doi.org/10.3390/biom13030483.

[15] Guañabens N, Gifre L, Peris P. The role of Wnt signaling and sclerostin in the pathogenesis of glucocorticoid-induced osteoporosis. Current Osteoporosis Reports. 2014; 12: 90–97. https://doi.org/10.1007/s11914-014-0197-0.

[16] Ahamad S, Saquib M, Hussain MK, Bhat SA. Targeting Wnt signaling pathway with small-molecule therapeutics for treating osteoporosis. Bioorganic Chemistry. 2025; 156: 108195. https://doi.org/10.1016/j.bioorg.2025.108195.

[17] Pan F, Huang K, Dai H, Sha C. PHF8 promotes osteogenic differentiation of BMSCs in old rat with osteoporosis by regulating Wnt/β-catenin pathway. Open Life Sciences. 2022; 17: 1591–1599. https://doi.org/10.1515/biol-2022-0523.

[18] Correa D, Almirall A, García-Carrodeguas R, dos Santos LA, De Aza AH, Parra J, *et al*. β-Dicalcium silicate-based cement: synthesis, characterization and *in vitro* bioactivity and biocompatibility studies.

Journal of Biomedical Materials Research. Part A. 2014; 102: 3693–3703. https://doi.org/10.1002/jbm.a.35041.

[19] Zuleta F, Murciano A, Gehrke SA, Maté-Sánchez de Val JE, Calvo-Guirado JL, De Aza PN. A New Biphasic Dicalcium Silicate Bone Cement Implant. Materials. 2017; 10: 758. https://doi.org/10.3390/ma10070758.

[20] Ruolan W, Liangjiao C, Longquan S. The mTOR/ULK1 signaling pathway mediates the autophagy-promoting and osteogenic effects of dicalcium silicate nanoparticles. Journal of Nanobiotechnology. 2020; 18: 119. https://doi.org/10.1186/s12951-020-00663-w.

[21] Sun J, Wei L, Liu X, Li J, Li B, Wang G, *et al*. Influences of ionic dissolution products of dicalcium silicate coating on osteoblastic proliferation, differentiation and gene expression. Acta Biomaterialia. 2009; 5: 1284–1293. https://doi.org/10.1016/j.actbio.2008.10.011.

[22] Zhong W, Li X, Pathak JL, Chen L, Cao W, Zhu M, *et al*. Dicalcium silicate microparticles modulate the differential expression of circRNAs and mRNAs in BMSCs and promote osteogenesis via circ_1983-miR-6931-Gas7 interaction. Biomaterials Science. 2020; 8: 3664–3677. https://doi.org/10.1039/d0bm00459f.

[23] Li HW, Sun JY. Effects of dicalcium silicate coating ionic dissolution products on human mesenchymal stem-cell proliferation and osteogenic differentiation. The Journal of International Medical Research. 2011; 39: 112–128. https://doi.org/10.1177/147323001103900114.

[24] Lin K, Xia L, Li H, Jiang X, Pan H, Xu Y, *et al*. Enhanced osteoporotic bone regeneration by strontium-substituted calcium silicate bioactive ceramics. Biomaterials. 2013; 34: 10028–10042. https://doi.org/10.1016/j.biomaterials.2013.09.056.

[25] Luo Q, Li X, Zhong W, Cao W, Zhu M, Wu A, *et al*. Dicalcium silicate-induced mitochondrial dysfunction and autophagy-mediated macrophagic inflammation promotes osteogenic differentiation of BMSCs. Regenerative Biomaterials. 2021; 9: rbab075. https://doi.org/10.1093/rb/rbab075.

[26] Lai S, Chen L, Cao W, Cui S, Li X, Zhong W, *et al*. Dicalcium Silicate Induced Proinflammatory Responses through TLR2-Mediated NF-κB and JNK Pathways in the Murine RAW 264.7 Macrophage Cell Line. Mediators of Inflammation. 2018; 2018: 8167932. https://doi.org/10.1155/2018/8167932.

[27] Kharode YP, Sharp MC, Bodine PV. Utility of the ovariectomized rat as a model for human osteoporosis in drug discovery. Methods in Molecular Biology. 2008; 455: 111–124. https://doi.org/10.1007/978-1-59745-104-8_8.

[28] Gu C, Zhou Q, Hu X, Ge X, Hou M, Wang W, *et al*. Melatonin rescues the mitochondrial function of bone marrow-derived mesenchymal stem cells and improves the repair of osteoporotic bone defect in ovariectomized rats. Journal of Pineal Research. 2024; 76: e12924. https://doi.org/10.1111/jpi.12924.

[29] Zhao B, Peng Q, Wang D, Zhou R, Wang R, Zhu Y, *et al*. Leonurine Protects Bone Mesenchymal Stem Cells from Oxidative Stress by Activating Mitophagy through PI3K/Akt/mTOR Pathway. Cells. 2022; 11: 1724. https://doi.org/10.3390/cells11111724.

[30] Zhou C, Hu G, Li Y, Zheng S. Polydatin accelerates osteoporotic bone repair by inducing the osteogenesis-angiogenesis coupling of bone marrow mesenchymal stem cells via the PI3K/AKT/GSK-3β/β-catenin pathway. International Journal of Surgery. 2025; 111: 411–425. https://doi.org/10.1097/js9.0000000000002075.

[31] Majidinia M, Sadeghpour A, Yousefi B. The roles of signaling pathways in bone repair and regeneration. Journal of Cellular Physiology. 2018; 233: 2937–2948. https://doi.org/10.1002/jcp.26042.

[32] Patel D, Wairkar S. Bone regeneration in osteoporosis: opportunities and challenges. Drug Delivery and Translational Research. 2023; 13: 419–432. https://doi.org/10.1007/s13346-022-01222-6.

[33] Falguera Uceda MI, Sánchez-Casanova S, Escudero-Duch C, Vilaboa N. A Narrative Review of Cell-Based Approaches for Cranial Bone Regeneration. Pharmaceutics. 2022; 14: 132. https://doi.org/10.3390/pharmaceutics14010132.

[34] Rosset P, Deschaseaux F, Layrolle P. Cell therapy for bone repair. Orthopaedics & Traumatology, Surgery & Research: OTSR. 2014; 100: S107–S112. https://doi.org/10.1016/j.otsr.2013.11.010.

[35] Safarova Y, Umbayev B, Hortelano G, Askarova S. Mesenchymal stem cells modifications for enhanced bone targeting and bone regeneration. Regenerative Medicine. 2020; 15: 1579–1594. https://doi.org/10.2217/rme-2019-0081.

[36] Rossi N, Hadad H, Bejar-Chapa M, Peretti GM, Randolph MA, Redmond RW, *et al*. Bone Marrow Stem Cells with Tissue-Engineered Scaffolds for Large Bone Segmental Defects: A Systematic Review. Tissue Engineering. Part B, Reviews. 2023; 29: 457–472. https://doi.org/10.1089/ten.TEB.2022.0213.

[37] Theodosaki AM, Tzemi M, Galanis N, Bakopoulou A, Kotsiomiti E, Aggelidou E, *et al*. Bone Regeneration with Mesenchymal Stem Cells in Scaffolds: Systematic Review of Human Clinical Trials. Stem Cell Reviews and Reports. 2024; 20: 938–966. https://doi.org/10.1007/s12015-024-10696-5.

[38] Primus CM, Tay FR, Niu LN. Bioactive tri/dicalcium silicate cements for treatment of pulpal and periapical tissues. Acta Biomaterialia. 2019; 96: 35–54. https://doi.org/10.1016/j.actbio.2019.05.050.

[39] Chen CC, Ho CC, David Chen CH, Wang WC, Ding SJ. *In vitro* bioactivity and biocompatibility of dicalcium silicate cements for endodontic use. Journal of Endodontics. 2009; 35: 1554–1557. https://doi.org/10.1016/j.joen.2009.08.006.

[40] Prati C, Gandolfi MG. Calcium silicate bioactive cements: Biological perspectives and clinical applications. Dental Materials: Official Publication of the Academy of Dental Materials. 2015; 31: 351–370. https://doi.org/10.1016/j.dental.2015.01.004.

[41] Wang L, Ruan M, Bu Q, Zhao C. Signaling Pathways Driving MSC Osteogenesis: Mechanisms, Regulation, and Translational Applications. International Journal of Molecular Sciences. 2025; 26: 1311. https://doi.org/10.3390/ijms26031311.

[42] Zhang DH, Shao J. Research Progress of Basing on Wnt/β-Catenin Pathway in the Treatment of Bone Tissue Diseases. Tissue Engineering. Part B, Reviews. 2025; 31: 555-565. https://doi.org/10.1089/ten.teb.2024.0170.

[43] Kang S, Bennett CN, Gerin I, Rapp LA, Hankenson KD, Macdougald OA. Wnt signaling stimulates osteoblastogenesis of mesenchymal precursors by suppressing CCAAT/enhancer-binding protein alpha and peroxisome proliferator-activated receptor gamma. The Journal of Biological Chemistry. 2007; 282: 14515–14524. https://doi.org/10.1074/jbc.M700030200.

[44] Muruganandan S, Roman AA, Sinal CJ. Adipocyte differentiation of bone marrow-derived mesenchymal stem cells: cross talk with the osteoblastogenic program. Cellular and Molecular Life Science: CMIS. 2009; 66: 236–253. https://doi.org/10.1007/s00018-008-8429-z.

[45] Shen G, Ren H, Shang Q, Zhao W, Zhang Z, Yu X, *et al*. Foxf1 knockdown promotes BMSC osteogenesis in part by activating the Wnt/β-catenin signalling pathway and prevents ovariectomy-induced bone loss. EBioMedicine. 2020; 52: 102626. https://doi.org/10.1016/j.ebiom.2020.102626.

Editor's note: The Scientific Editor responsible for this paper was Christine Hartmann.

Received: 23rd May 2025; **Accepted**: 2nd December 2025; **Published**: 31st December 2025